

Automatic Pan–Tilt Camera Control for Learning Dirichlet Process Gaussian Process (DPGP) Mixture Models of Multiple Moving Targets

Hongchuan Wei¹, Pingping Zhu¹, Member, IEEE, Miao Liu², Jonathan P. How³, Fellow, IEEE, and Silvia Ferrari⁴, Senior Member, IEEE

Abstract—Information value functions based on the Kullback–Leibler (KL) divergence have been shown the most effective for planning sensor measurements by means of greedy strategies. The problem of optimizing information value over a finite time horizon to date has been considered computationally intractable and, as proven here, is NP-hard. This paper presents new information value functions that are additive and can be optimized efficiently over time by deriving a lower bound of the KL divergence. Combined with a convex approximation of the sensor field of view, these information value functions can be used to obtain real-time sensor control by a lexicographic approach, and to derive performance guarantees. Numerical and experimental results on pedestrian data show that the lexicographic control system significantly improves target modeling and prediction performance when compared to existing algorithms.

Index Terms—Active sensing, automatic control, camera, information value, lexicographic control, multiobjective optimization (MO), target, tracking.

I. INTRODUCTION

THE problem of learning the behavior of many moving targets by means of a reconfigurable sensor, such as a camera, is relevant to a wide range of applications, including security and surveillance [1], [2], environmental monitoring [3], and tracking of endangered species [4]. In many of these applications, little or no prior information exists about the target behavior or the number of targets that is present in the region of interest (ROI). Also, the number of targets and possible behaviors may change rapidly over time as new targets arrive and old targets leave the

Manuscript received March 15, 2017; revised March 17, 2017 and December 17, 2017; accepted February 7, 2018. Date of publication June 21, 2018; date of current version December 24, 2018. This work was supported by the Office of Naval Research MURI Grant N000141110688. Recommended by Associate Editor G. Pillonetto. (Corresponding author: Silvia Ferrari.)

H. Wei is with the Mechanical Engineering and Materials Science, Duke University, Durham, NC 27708 USA (e-mail: hongchuan.wei@duke.edu).

P. Zhu and S. Ferrari are with the Sibley School of Mechanical and Aerospace Engineering, Cornell University, Ithaca, NY 14853 USA (e-mail: pingping.zhu@cornell.edu; sferrari@cornell.edu).

M. Liu is with the IBM T. J. Watson Research Center, Yorktown Heights, NY 10598 USA (e-mail: miao.liu1@ibm.com).

J. P. How is with the Massachusetts Institute of Technology, Cambridge, MA 02139 USA (e-mail: jhow@mit.edu).

Color versions of one or more of the figures in this paper are available online at <http://ieeexplore.ieee.org>.

Digital Object Identifier 10.1109/TAC.2018.2849584

ROI. When the sensor remains in place over long periods of time, it produces a growing database of target measurements that can cause parametric statistical learning methods to fail to accurately predict/track/model target behaviors due to overfitting or underfitting. Bayesian nonparametric models, and in particular Dirichlet process Gaussian process (DPGP) mixtures, have been shown very effective at learning models of multiple mobile targets, such as pedestrians [5], urban traffic [6], and migrating animals [7], exclusively from data. The advantages of DPGP mixtures over other probabilistic models are that they do not require a parametric form of target dynamics *a priori*, and they adjust the dimensionality of the model based on data to avoid overfitting and underfitting [8]–[10].

Automatic control is crucial to sensors tasked with observing multiple targets using a bounded field of view (FOV) because the set of useful measurements far exceeds the measurements that can be obtained in practice [2], [11]. The FOV geometry and sensor kinematic constraints must both be taken into account to guarantee that a desired FOV placement is realizable, or that targets are observed for a sufficient period of time before they leave the sensor workspace [12], [13]. It was recently shown that the value of camera measurements used for learning a DPGP mixture model (MM) can be represented in closed form by an information value function derived from the expected Kullback–Leibler divergence (EKLD) [14]. However, as proven in Section IV-A, the problem of optimizing the DPGP EKLD over a finite time horizon, subject to the FOV and kinematic constraints, is NP-hard. Therefore, previous methods sought greedy or approximate solutions that lacked reachability and performance guarantees [14]–[18].

This paper presents an approach for casting the camera control problem as a multiobjective optimization (MO) problem that can be solved and implemented in real time. The approach is based on new theoretical developments that include the derivation of a cumulative DPGP KL information value function (see Section IV-A), and an additive lower bound that can be optimized in place of the cumulative DPGP KL function (see Theorem 3). The MO control problem is further simplified by obtaining a linear approximation of the FOV constraints that guarantees target observability by means of a convex potential function in lieu of expensive disjunctions of nonlinear inequality constraints (see Section V-A). As a result, the lexicographic solution presented in Section V-B can be obtained in

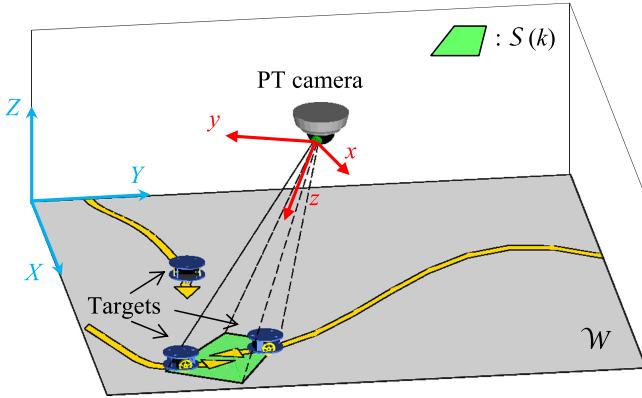


Fig. 1. PT camera observing three mobile targets in \mathcal{W} .

polynomial time and is accompanied by both reachability and performance guarantees. Studies based on real indoor pedestrian datasets obtained from two MIT buildings [10] show that the lexicographic control method can be implemented in real time to improve camera performance by well over 100% compared to algorithms based on greedy entropy [19], greedy KL divergence [20], potential field [21], patrol [22], and randomly exploring trees [17].

II. PROBLEM FORMULATION AND ASSUMPTIONS

This paper considers the problem of controlling a pan-tilt (PT) camera used to learn the kinematics of multiple mobile targets traversing a workspace or ROI, $\mathcal{W} \subset \mathbb{R}^2$. It is assumed that the target kinematics in \mathcal{W} are to be learned entirely from camera measurements, and that each target obeys a time-invariant nonlinear ordinary differential equation

$$\dot{\mathbf{x}}_j(t) = \mathbf{f}_i[\mathbf{x}_j(t)] \triangleq \mathbf{v}_j(t), \quad j = 1, \dots, N(t) \quad (1)$$

where $\mathbf{x}_j \in \mathcal{W}$ and $\mathbf{v}_j \in \mathbb{R}^2$ denote the position and velocity of the j th target in inertial XY -coordinate frame, respectively, and $\mathcal{I}(t)$ denotes the target index set at time t . The vector function $\mathbf{f}_i : \mathbb{R}^2 \rightarrow \mathbb{R}^2$, referred to as a *velocity field* (VF), is drawn from a set of continuously differentiable VFs, $\mathcal{F} = \{\mathbf{f}_1, \dots, \mathbf{f}_M\}$, where both \mathbf{f}_i and M are unknown *a priori*. The number of VFs, M , and the number of targets, N , are both unknown and change over time, as targets enter and exit the workspace. Since multiple targets may be characterized by the same kinematics, N is not necessarily equal to M .

Assuming a constant sampling interval Δt , at any discrete time k the camera obtains target position and velocity measurements using simple computer vision algorithms [23] applied to consecutive frames obtained from the FOV projection onto \mathcal{W} , denoted by the compact subset $\mathcal{S}(k) \subset \mathcal{W}$, and illustrated in Fig. 1. The camera obeys a nonlinear measurement model with additive Gaussian noise

$$\mathbf{z}_j(k) = \begin{cases} \mathbf{y}_j(k) + \mathbf{n}(k), & \text{if } \mathbf{x}_j(k) \in \mathcal{S}(k) \\ \emptyset, & \text{if } \mathbf{x}_j(k) \notin \mathcal{S}(k) \end{cases} \quad (2)$$

where

$$\mathbf{y}_j(k) = \mathbf{h}[\mathbf{x}_j(k), \mathbf{v}_j(k)] \quad (3)$$

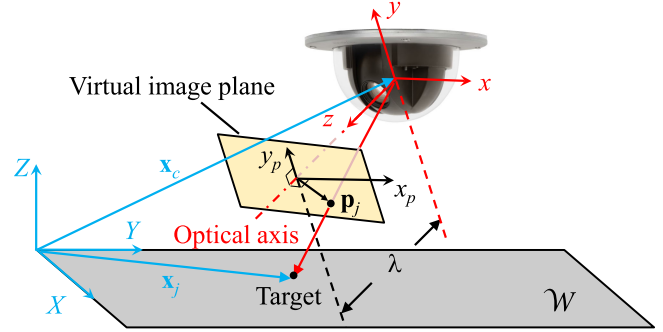


Fig. 2. Pinhole camera model.

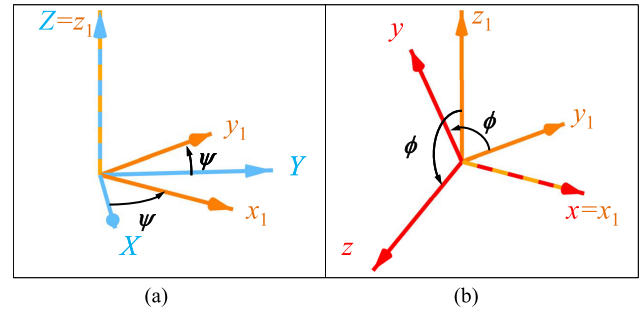


Fig. 3. Sequence of yaw and roll Euler angle rotations comprised of the camera pan angle ψ and tilt angle ϕ , respectively.

and the noise vector $\mathbf{n} \in \mathbb{R}^4$ is a white, zero-mean Gaussian random sequence with a known and symmetric covariance matrix \mathbf{Q} . The form of the nonlinear measurement model, described by the vector function $\mathbf{h}[\cdot]$, is obtained from first principles in the remainder of this section.

Based on the pinhole camera model [24], the camera lens is symmetric about a so-called *optical axis*, and images of \mathcal{S} are projected onto a two-dimensional (2-D) *virtual image plane* perpendicular to the optical axis and located at a distance λ from the pinhole [25], [26]. The distance λ between the virtual image plane and the pinhole is also known as focal length [27]. A camera-fixed frame of reference is defined by placing the origin at the pinhole (see Fig. 2), aligning the z -axis with the optical axis and the x -axis parallel to the XY plane, and obtaining the y -axis by the right-hand rule. Then, the camera pan and tilt angles can be represented by the Euler angles known as yaw (ψ) and roll (ϕ) angles, respectively, and illustrated in Fig. 3. These two Euler angles are defined by two successive right-hand rotations: a rotation by an angle ψ about the Z -axis, leading to the intermediate frame (x_1, y_1, z_1) [see Fig. 3(a)], followed by a rotation by an angle ϕ about the x_1 -axis, leading to the camera-fixed frame (x, y, z) [see Fig. 3(b)]. Then, any vector in inertial frame can be resolved into the camera-fixed frame by the following transformation:

$$\mathbf{x}|_{\text{camera}} = \mathbf{R}_\phi \mathbf{R}_\psi \mathbf{x}|_{\text{inertial}} \quad (4)$$

defined in terms of the Euler rotation matrices

$$\mathbf{R}_\phi \triangleq \begin{bmatrix} 1 & 0 & 0 \\ 0 & \cos \phi & \sin \phi \\ 0 & -\sin \phi & \cos \phi \end{bmatrix}, \quad \mathbf{R}_\psi \triangleq \begin{bmatrix} \cos \psi & \sin \psi & 0 \\ -\sin \psi & \cos \psi & 0 \\ 0 & 0 & 1 \end{bmatrix}.$$

Consider now a 2-D frame of reference (x_p, y_p) embedded in the virtual image plane, such that its origin lies at the intersection between the virtual image plane and the optical axis, the x_p -axis is chosen parallel to XY plane, and the y_p -axis is orthogonal to the x_p -axis and the optical axis, as shown in Fig. 2. The position of the target with respect to the camera-fixed frame is given by

$$\mathbf{q}_j = \mathbf{R}_\phi \mathbf{R}_\psi ([\mathbf{x}_j^T \ 0]^T - \mathbf{x}_c) \triangleq [q_x \ q_y \ q_z]^T \quad (5)$$

where $\mathbf{x}_c = [x_c \ y_c \ z_c]^T$ is the pinhole position with respect to the inertial frame (see Fig. 2). Then, it can be easily shown that the projection of a target position \mathbf{x}_j onto the virtual image plane with respect to the (x_p, y_p) -frame is

$$\mathbf{p}_j = \lambda [q_x/q_z \ q_y/q_z]^T \triangleq [p_x \ p_y]^T. \quad (6)$$

The projection of the target velocity \mathbf{v}_j onto the (moving) camera virtual image plane is found by differentiating both sides of (6) with respect to time

$$\dot{\mathbf{p}}_j = [\dot{p}_x \ \dot{p}_y]^T = \mathbf{H} \begin{bmatrix} \mathbf{R}_\phi \mathbf{R}_\psi & \mathbf{0} \\ \mathbf{0} & -\mathbf{R}_\phi \end{bmatrix} [\dot{\mathbf{x}}_j^T \ 0 \ \dot{\phi} \ 0 \ \dot{\psi}]^T \quad (7)$$

where

$$\mathbf{H} \triangleq \begin{bmatrix} -\frac{\lambda}{q_z} & 0 & \frac{p_x}{q_z} & \frac{p_x p_y}{\lambda} & -\frac{\lambda^2 + p_y^2}{\lambda} & p_y \\ 0 & -\frac{\lambda}{q_z} & \frac{p_y}{q_z} & \frac{\lambda^2 + p_x^2}{\lambda} & -\frac{p_x p_y}{\lambda} & -p_x \end{bmatrix} \quad (8)$$

is the image Jacobian matrix, derived in [24].

Using the above projections and transformations, the vector function $\mathbf{h}[\cdot]$ in the measurement equation (2) is derived by recognizing that the camera output vector \mathbf{y}_j consists of the target position and velocity in the (x_p, y_p) -frame

$$\mathbf{y}_j(k) = \mathbf{h}[\mathbf{x}_j(k), \mathbf{v}_j(k)] = [\mathbf{p}_j^T(k) \ \dot{\mathbf{p}}_j^T(k)]^T \quad (9)$$

and, thus, the functional elements of $\mathbf{h}[\cdot]$ are given by (6) and (7), completing the definition of the PT camera measurement and output equations (2) and (3).

The PT camera kinematic equations can be obtained from the kinematic constraints on the motor and pinhole or lens movements, which determine the motion constraints on the FOV \mathcal{S} . Furthermore, the FOV shape changes based on the orientation of the camera with respect to \mathcal{W} . Let $\mathbf{s} = [\psi \ \phi \ \dot{\psi} \ \dot{\phi}]^T$ denote the dynamic state of the camera. In this paper, it is assumed that the camera kinematics are linear [28] and the camera control input, $\mathbf{u} = [u_1 \ u_2]^T$, consists of two voltage levels that, applied to the motors, can independently adjust the pan and tilt angles [29]. Then, the camera kinematic equation can be expressed by a difference equation in the state-space form

$$\mathbf{s}(k+1) = \mathbf{A}\mathbf{s}(k) + \mathbf{B}\mathbf{u}(k) \quad (10)$$

where

$$\mathbf{A} = \begin{bmatrix} 1 & 0 & \Delta t & 0 \\ 0 & 1 & 0 & \Delta t \\ 0 & 0 & 1 & 0 \\ 0 & 0 & 0 & 1 \end{bmatrix}, \quad \mathbf{B} = \begin{bmatrix} 0 & 0 \\ 0 & 0 \\ b_1 & 0 \\ 0 & b_2 \end{bmatrix} \quad (11)$$

and b_1 and b_2 are two constant motor parameters [30].

In addition to the kinematic constraint (10), the camera state and control must also obey inequality constraints that reflect physical bounds imposed by the instrumentation. The pan and tilt angles are constrained to the ranges $\psi \in [0, 2\pi)$ and $\phi \in [\pi/2, \pi]$, and the pan and tilt angular velocities are bounded by the constants $\dot{\psi}_{\max}$ and $\dot{\phi}_{\max}$, respectively. Then, by normalizing the camera input voltages such that their upper bounds are equal to one, the full set of camera inequality constraints can be expressed as

$$\begin{cases} \mathbf{b}_1 \leq \mathbf{s} \leq \mathbf{b}_2 \\ |\mathbf{u}| \leq \mathbf{1}_2 \end{cases} \quad (12)$$

where \leq denotes elementwise inequalities, $\mathbf{b}_1 = [0 \ \pi/2 \ -\dot{\psi}_{\max} \ -\dot{\phi}_{\max}]^T$, $\mathbf{b}_2 = [2\pi \ \pi \ \dot{\psi}_{\max} \ \dot{\phi}_{\max}]^T$, $\mathbf{1}_n$ denotes an $n \times 1$ vector of ones, and input scaling coefficients have been absorbed into the matrix \mathbf{B} in (11).

The automatic control problem addressed in this paper is to determine a control sequence $\{\mathbf{u}^*(\ell)\}_{\ell=k, \dots, k_f}$ that at any time k optimizes the expected PT camera performance over a finite time horizon $[k, k_f]$. The PT camera performance is represented by the information value of future target measurements, in the form (2), and is to be maximized subject to the PT camera kinematic equation (10) and inequality constraints (12), and FOV geometric constraint $\mathcal{S}(k)$. The length of the time horizon $T = (k_f - k)$ is determined by the time it takes to update a probabilistic model of the target kinematics (1) based on all measurements obtained up to time k , using the Bayesian nonparametric approach reviewed in Section III.

III. BACKGROUND ON BAYESIAN NONPARAMETRIC MODELS AND INFORMATION VALUE

Several authors have recently shown that the kinematics of an unknown number of mobile targets in the form (1) can be learned entirely from data using DPGP MMs adapted automatically to learn the number and form of target VFs from noisy measurements [5], [9], [10], [31]. Because the number of targets, $N(t)$, and the number of VFs, $M(t)$, are both unknown and not necessarily equal, the target-VF associations are modeled by a set of hidden discrete random variables, $G_j \in \{1, \dots, M\}$, for $j \in \mathcal{I}$, with a distribution of mixture weights, $\boldsymbol{\pi} = [\pi_1 \ \dots \ \pi_M]^T$, modeled via DP.

A multioutput GP defines a multivariate distribution over functions, $P(\mathbf{f}_i)$, for $\mathbf{f}_i : \mathcal{W} \rightarrow \mathbb{R}^d$, where, in this paper, $d = 2$, and $i = 1, \dots, M$ [9]. Let $F = \{\mathbf{f}_i(\mathbf{x}_1), \dots, \mathbf{f}_i(\mathbf{x}_n) | \mathbf{x}_j \in \mathcal{W}\}$ be a set of vector function values obtained at n points in \mathcal{W} . Then, $P(\mathbf{f}_i)$ is a multioutput Gaussian process if for any finite set $\{\mathbf{x}_1, \dots, \mathbf{x}_n\}$ the distribution $P(F)$ is a joint multivariate Gaussian distribution. Now, let $\boldsymbol{\theta}_i(\mathbf{x}_j) \triangleq \mathbb{E}_{\mathbf{v}_j}[\mathbf{f}_i(\mathbf{x}_j)]$ denote the GP mean, and $\boldsymbol{\Psi}_i(\mathbf{x}_j, \mathbf{x}'_j) \triangleq \mathbb{E}_{\mathbf{v}_j, \mathbf{v}'_j} \{[\mathbf{f}_i(\mathbf{x}_j) - \boldsymbol{\theta}_i(\mathbf{x}_j)][\mathbf{f}_i(\mathbf{x}'_j) - \boldsymbol{\theta}_i(\mathbf{x}'_j)]^T\}$ denote the GP covariance, where $\mathbb{E}[\cdot]$ is the expectation operator [32]. Together, $\boldsymbol{\theta}_i$ and $\boldsymbol{\Psi}_i$ fully specify the i th GP. For simplicity, it is assumed that all the GPs share the same known covariance matrix $\boldsymbol{\Psi}$.

Under proper assumptions [14], the following DPGP MM:

$$\begin{aligned} \{\theta_i, \pi\} &\sim \text{DP}(\alpha, \text{GP}(\mathbf{0}, \Psi)), i = 1, \dots, \infty \\ G_j &\sim \text{Cat}(\pi), j \in \mathcal{I} \\ \mathbf{f}_{G_j}(\mathbf{x}) &\sim \text{GP}(\theta_{G_j}, \Psi), \mathbf{x} \in \mathcal{W}, j \in \mathcal{I} \end{aligned} \quad (13)$$

can be used to describe the target kinematics in (1) from the position and velocity measurements (2), where ‘‘Cat’’ denotes the categorical distribution, α is a positive real number, and ‘‘ \sim ’’ denotes ‘‘is distributed as.’’ Each VF is modeled as a Gaussian process, and the target–VF association is modeled by π .

Recent works [14], [20], [33] have shown that, at time k , the information value of a (future) measurement in the form (2) can be estimated by an expected information theoretic function, such as the EKLD, derived from the DPGP model. Because traditional information theoretic functions are defined in terms of probability distributions, in [14] Wei *et al.* proposed a collocation-point method to derive computationally tractable DPGP information theoretic functions. The approach consists of evaluating the VFs in \mathcal{F} at L collocation points distributed on a uniform grid in \mathcal{W} , and denoted by $\{\xi_l \in \mathcal{W} | l = 1, \dots, L\}$. From finite difference analysis [34], every VF $\mathbf{f}_i(\cdot)$ learned by the DPGP can be approximated by the $(2L \times 1)$ random vector

$$\mathbf{v}_i \triangleq [\mathbf{f}_i(\xi_1)^T \quad \dots \quad \mathbf{f}_i(\xi_L)^T]^T. \quad (14)$$

By arranging all M VFs approximations into a $2LM \times 1$ vector, $\mathbf{v} \triangleq [\mathbf{v}_1^T \quad \dots \quad \mathbf{v}_M^T]^T$, a finite-difference approximation is obtained for the set of VFs \mathcal{F} learned by the DPGP up to time k .

Then, the KL divergence between two multivariate distributions, $p(\mathbf{v})$ and $q(\mathbf{v})$, of the random vector $\mathbf{v} \in \mathbb{R}^{2LM}$, defined as

$$D(p(\mathbf{v}) \| q(\mathbf{v})) = \int_{\mathbb{R}^{2LM}} p(\mathbf{v}) \ln \frac{p(\mathbf{v})}{q(\mathbf{v})} d\mathbf{v} \quad (15)$$

can be used to represent the information value associated with the change in distribution for \mathbf{v} . Let the set of measurements obtained from an initial time ($\ell = 1$) up to but not including time k be denoted by $Z(1, k) = \{\mathbf{z}_j(\ell) | j \in \mathcal{I}(\ell), 1 \leq \ell < k\}$, where $\mathbf{z}_j(\ell)$ obeys (2) for all j and ℓ . The information value associated with the *next* measurement $\mathbf{z}_j(k)$, resulting in a change in the distribution of \mathbf{v} , can be represented by the KL divergence between the prior and posterior distributions

$$\begin{aligned} &D(p(\mathbf{v} | \mathbf{z}_j(k), Z(1, k)) \| p(\mathbf{v} | Z(1, k))) \\ &= \int_{\mathbb{R}^{2LM}} p(\mathbf{v} | \mathbf{z}_j(k), Z(1, k)) \ln \frac{p(\mathbf{v} | \mathbf{z}_j(k), Z(1, k))}{p(\mathbf{v} | Z(1, k))} d\mathbf{v}. \end{aligned} \quad (16)$$

Because the posterior distribution of \mathbf{v} is unknown before the values of \mathbf{z}_j and G_j are obtained by the camera, the KL divergence in (16) is estimated by taking the expectation with respect to these two random variables

$$\begin{aligned} &\hat{D}(p(\mathbf{v} | \mathbf{z}_j(k), Z(1, k)) \| p(\mathbf{v} | Z(1, k))) \\ &= \mathbb{E}_{\mathbf{z}_j(k)} \{ \mathbb{E}_{G_j(k)} \{ D(p(\mathbf{v} | \mathbf{z}_j(k), Z(1, k)) \| p(\mathbf{v} | Z(1, k))) \} \} \triangleq \hat{D}(\mathbf{v}; \mathbf{z}_j(k)) \end{aligned} \quad (17)$$

resulting in the EKLD of measurement $\mathbf{z}_j(k)$.

IV. ADDITIVE BAYESIAN NONPARAMETRIC INFORMATION VALUE

Previous work on Bayesian nonparametric (BNP) information value and related control methods have focused on greedy strategies that consider the information value of the next *single* sensor measurement, e.g. the EKLD information value function in (17), and that do not account for the camera kinematic constraints [14], [20], [33], [35]. However, in real-world applications, the camera kinematic and FOV constraints (see Section II) impose real limitations on possible measurement realizations. For example, during the time it takes the camera to reposition its FOV targets may have moved elsewhere and, because their behavior is unknown or highly uncertain, they may have left the workspace altogether. This section obtains a closed-form representation of the camera information value that is additive over time and computationally tractable, so as to capture and optimize the camera ability to build the target models in (1) over a finite time horizon. As shown in Section IV-A, the DPGPEKLD is not additive, and its optimization is proven NP-hard (see Section IV-A). Thus, a new information value function that is additive and tractable is obtained from the EKLD lower bound derived in Section IV-B. Based on this result, the constrained camera control problem is cast as an MO optimization problem that can be solved efficiently by the lexicographic approach presented in Section V.

A. Cumulative BNP Information Value Optimization

Consider a finite time horizon of T time steps, where T is a finite and known positive integer. Now, let $Z_j(k_1, k_2) = \{\mathbf{z}_j(\ell) | j \in \mathcal{I}(\ell); k_1 \leq \ell < k_2\}$ denote the set of measurements obtained from the j th target between time steps k_1 and k_2 , and let $Z(k_1, k_2) \triangleq \cup_j Z_j(k_1, k_2)$ denote the set of all measurements obtained between k_1 and k_2 . Then, at any time k , the cumulative DPGP information value of the j th target measurements obtained over the T time horizon can be represented by the EKLD of the measurement set $Z_j(k, k_f)$, where $k_f = (k + T)$, such that from (17)

$$\begin{aligned} \hat{D}(\mathbf{v}; Z_j(k, k_f)) &= \mathbb{E}_{Z_j(k, k_f)} \{ \mathbb{E}_{G_j(k)} \{ D(p(\mathbf{v} | Z_j(k, k_f)) \\ &\quad \cup Z(1, k)) \| p(\mathbf{v} | Z(1, k)) \} \} \end{aligned} \quad (18)$$

where it is assumed that the target–VF association G_j remains constant from k to k_f .

Because the EKLD of any two random variables X and Y can be expressed in terms of mutual information, as follows:

$$I(X; Y) \triangleq \mathbb{E}_Y \{ D[p(X|Y) \| p(X)] \} \quad (19)$$

the cumulative EKLD in (18) can be written as

$$\hat{D}(\mathbf{v}; Z_j(k, k_f)) = \sum_{i=1}^M w_{ij} I(\mathbf{v}_i; Z_j(k, k_f)) \quad (20)$$

where w_{ij} denotes the posterior probability of event $\{G_j = i\}$, and \mathbf{v}_i is defined in (14). Let $\bar{Z}_j(1, k)$ denote the complement set of $Z_j(1, k)$ in $Z(1, k)$. Then, from Bayes’ rule, the posterior

probability of a target–VF association event is

$$w_{ij} = \frac{\pi_i \cdot p(Z_j(1, k) | \bar{Z}_j(1, k), G_j = i)}{\sum_{i=1}^M \pi_i \cdot p(Z_j(1, k) | \bar{Z}_j(1, k), G_j = i)} \quad (21)$$

where $\pi_i = p(G_j = i)$ is the prior probability that the j th target follows the i th VF, and all likelihood functions in (21) can be obtained from the cross-covariance matrix of the GP regression, as shown in [14] and [36].

We will now show that the computational complexity of maximizing the cumulative EKLD in (20) subject to the camera kinematic constraints (10)–(12) and the bounded FOV (2) is NP-hard. From (20) and (21), maximizing the cumulative EKLD with respect to future measurements is equivalent to maximizing the mutual information $I(\mathbf{v}_i; Z_j(k, k_f))$ since the posterior w_{ij} is independent of $Z_j(k, k_f)$. From the properties of mutual information [37], $I(X; Y) = H(X) - H(X|Y)$ for any two random variables X and Y , where $H(X)$ denotes the entropy of X , and $H(X|Y)$ denotes the conditional entropy of X given Y . The computational complexity of determining entropy bounds is given by the following Lemma (from [38]).

Lemma 1: Given rational number n and rational covariance matrix Σ over a set of Gaussian random variables S , deciding whether there exists a subset $A \subset S$ of cardinality $|A| = d$ such that $H(A) \geq n$ is NP-complete.

From the above Lemma, the computational complexity of determining bounds on mutual information is as follows.

Theorem 1: Given a rational number m and a rational covariance matrix Λ over a set of Gaussian random variables $V = S \cup U$, deciding whether there exists a subset $A \subset S$, where $|A| = d$, such that $I(A; U) \geq m$ is NP-complete.

Proof: Letting Q_1 and Q_2 denote the problems studied in Lemma 1 and Theorem 1, respectively, Q_2 can be shown NP-complete by the reducing Q_1 to Q_2 as follows. Consider a positive constant $\sigma_c < \sqrt{\lambda_{\min}(\Sigma)}$, where the smallest eigenvalue λ_{\min} of a covariance matrix is always positive. Then $\forall S, \exists U$ such that any random variable in V is multivariate Gaussian distributed with covariance matrix

$$\Lambda = \begin{bmatrix} \Sigma & \mathbf{I} \\ \mathbf{I} & (\Sigma - \sigma_c^2 \mathbf{I})^{-1} \end{bmatrix}. \quad (22)$$

The conditional distribution of S given U is a multivariate Gaussian distribution with covariance matrix $\sigma_c^2 \mathbf{I}$. Thus, the random variables in S are conditionally independent given U .

Now let $I(A; U) = H(A) - H(A|U)$, where $H(A)$ is maximized in Q_1 , and $H(A|U)$ can be shown constant as follows. Since $A \subset S$, all random variables in A also are conditionally independent given U and, thus, $H(A|U) = d \log(2\pi e \sigma_c^2) / 2$ is constant for known $|A| = d$. It also follows that maximizing $I(A; U)$ is equivalent to maximizing $H(A)$, thus the solution to Q_2 can be used as a black-box to solve Q_1 in polynomial steps and, since Q_1 is NP-complete, Q_2 is NP-hard. Furthermore, calculating $I(\cdot)$ for a set of Gaussian random variables requires polynomial time, therefore, Q_2 is NP-complete. ■

From Theorem 1, the complexity of optimizing the cumulative DPGP information value over a finite time horizon subject to the camera constraints is given by the following result.

Theorem 2: Determining the measurement set $Z_j(k, k_f)$ that maximizes the EKLD function, $\hat{D}(\mathbf{v}; Z_j(k, k_f))$ in (20), subject to the camera kinematic constraints (10)–(12) and bounded FOV (2), is NP-hard.

Proof: The proof shows that the constrained optimization of \hat{D} , denoted by Q_3 , contains the NP-complete problem Q_2 defined in Theorem 1 [39]. In particular, three restrictions are introduced to demonstrate that Q_2 is a special case of Q_3 . The first restriction to demonstrate that Q_2 is a special case of Q_3 . The first restriction $M = 1$ considers the case of a unique VF \mathbf{f}_1 associated with all N targets, such that $S = \{\mathbf{f}_1[\mathbf{x}_j(\ell)] \mid 1 \leq j \leq N, k \leq \ell \leq k_f\}$. The second restriction considers an FOV S sufficiently small to obtain one and only one target measurement \mathbf{z}_j at any time step k . It follows that $d = |Z_j(k, k_f)| = (k_f - k) = T$ in Q_2 . The third restriction is placed on the collocation points used to evaluate the DPGP EKLD, namely, considers one collocation point ξ_l . Then, $\mathbf{v} = \mathbf{v}_1 = \mathbf{f}_1(\xi_l)$, and the VF $\mathbf{f}_1[\cdot]$ specifies the set $U = \{\mathbf{f}_1(\xi_l) \mid 1 \leq l \leq L\}$. Because from (20) maximizing $\hat{D}(U; A)$ is equivalent to maximizing $I(U; A)$, and $I(U; A) = I(A; U)$, under the above restrictions Q_3 is equivalent to Q_2 and, since Q_2 is NP-complete, Q_3 is NP-hard. ■

In order to reduce the computational complexity of the above optimization problem, the following section derives a lower bound for the DPGP-EKLD that represents the camera worst case performance and is shown to be additive over time.

B. BNP Cumulative Information Value Lower Bound

Because the cumulative EKLD in (20) is a nonadditive function of the future measurements, $Z_j(k, k_f)$, maximizing \hat{D} is a combinatorial optimization problem. This section shows that the problem complexity can be greatly reduced by the following additive lower bound of the DPGP EKLD.

Theorem 3: Given a time horizon $[k, k_f]$, the cumulative DPGP EKLD function, $\hat{D}(\mathbf{v}; Z_j(k, k_f))$, in (20), is characterized by the lower bound, $\hat{D}_L(\mathbf{v}; Z_j(k, k_f))$, obtained from the discounted mutual information of every future measurement, $\mathbf{z}_j(\ell)$ ($\ell = k, \dots, k_f$), as follows:

$$\begin{aligned} \hat{D}(\mathbf{v}; Z_j(k, k_f)) &\geq \sum_{i=1}^M \sum_{\ell=k}^{k_f} w_{ij} (1 - \gamma) \gamma^{\ell-k} I(\mathbf{v}_i; \mathbf{z}_j(\ell)) \\ &\triangleq \hat{D}_L(\mathbf{v}; Z_j(k, k_f)) \end{aligned} \quad (23)$$

where $\gamma \in [0, 1)$ is a constant discount factor.

Proof: Let V , A_1 , and A_2 denote any three sets of random variables, and $A \triangleq A_1 \cup A_2$. Since $A_1, A_2 \subset A$, it follows from the properties of conditional entropy [37] that $H(V|A) \leq H(V|A_1)$ and $H(V|A) \leq H(V|A_2)$ and, also, for any constant $\gamma \in (0, 1)$, the following holds:

$$I(V; A) \geq \gamma I(V; A_1) + (1 - \gamma) I(V; A_2). \quad (24)$$

By induction, from the above inequality it also follows that

$$I(\mathbf{v}_i; Z_j(k, k_f)) \geq \sum_{\ell=k}^{k_f} (1 - \gamma) \gamma^{\ell-k} I(\mathbf{v}_i; \mathbf{z}_j(\ell)) \quad (25)$$

and, thus, substituting (25) in (20) yields the cumulative lower bound of the EKLD

$$\hat{D}(\mathbf{v}; Z_j(k, k_f)) \geq \sum_{i=1}^M \sum_{\ell=k}^{k_f} w_{ij} (1-\gamma) \gamma^{\ell-k} I(\mathbf{v}_i; \mathbf{z}_j(\ell)).$$

The information value function in (23) is evaluated using the DPGP mutual information and regression, as shown by (19), (21), and Section III (see [14] for more details).

V. LEXICOGRAPHIC MO CAMERA CONTROL METHOD

The new camera information value function in (23) can be viewed as the sum of multiple objective functions, each proportional to the mutual information representing the expected improvement of the i th VF brought about by a future measurement $\mathbf{z}_j(\ell)$ obtained from the j th target at time $\ell \geq k$. Thus, the automatic control problem formulated in Section II can be viewed as a constrained MO problem [40] comprised of MN objective functions to be optimized simultaneously subject to the dynamic and inequality constraints (10)–(12), and the geometric FOV constraints in (2). By solving the constrained MO problem over the finite time horizon $[k, k_f]$, the PT camera can be automatically controlled so as to obtain the most informative measurements for learning the target DPGP model hyperparameters $\{\boldsymbol{\theta}_i, \boldsymbol{\Psi}, \boldsymbol{\pi}\}$ in (13). As a result, many problems associated with greedy algorithms, such as local minima, are mitigated and the camera performance is significantly improved (see Section VI).

The lexicographic approach belongs to the class of methods with *a priori* articulation of preference, which assumes the objectives can be ranked in order of importance [41]. When compared to other methods in this class, such as weighted global criterion methods, the lexicographic approach avoids unfavorable local optima [42]. Also, the lexicographic approach is more computationally efficient than methods with *a posteriori* articulation of preference [43], and it does not require closeness between solutions as do methods without articulation of preference, such as compromise solutions methods [44]. The camera MO problem is cast in a form suitable to the lexicographic approach in Section V-A, and a solution method is presented in Section V-B along with theoretical results that include guarantees on the MO solution obtained by convex quadratic programming (QP).

A. MO Problem and Ordering of Objectives

The FOV geometric constraints in (2) can be formulated as a set of inequality constraints on the state and control by means of disjunction operators that significantly increase the complexity of the constrained optimization problem [45]–[47]. This paper presents an alternative approach that adjoins the FOV constraint to the objective function (23) by means of a convex potential function, $\mathbf{g} : \mathbb{R}^2 \rightarrow [0, 2\pi) \times [\pi/2, \pi]$, mapping any target position, \mathbf{x}_j , to pan and tilt angles that position the centroid of S

at \mathbf{x}_j , as follows:

$$\begin{bmatrix} \psi_j \\ \phi_j \end{bmatrix} = \begin{bmatrix} \tan^{-1} [(y_c - y_j)/(x_c - x_j)] \\ \pi - \tan^{-1} \left[\frac{\sqrt{(y_c - y_j)^2 + (x_c - y_j)^2}}{z_c} \right] \end{bmatrix} \triangleq \mathbf{g}(\mathbf{x}_j) \quad (26)$$

where \mathbf{x}_c is the pinhole position in inertial frame and the above transformation is obtained from (5) (see Section II). Then, the quadratic function

$$P(\mathbf{s}, \mathbf{x}_j) = 1 - \|\mathbf{U}\mathbf{s} - \mathbf{g}(\mathbf{x}_j)\|^2/h \quad (27)$$

is maximized to achieve $\mathbf{x}_j \in \mathcal{S}$ (time arguments omitted for brevity), where $\mathbf{U} \triangleq \begin{bmatrix} 1 & 0 & 0 & 0 \\ 0 & 1 & 0 & 0 \end{bmatrix}$, and $h > 0$ is a user-defined weight known as shape parameter.

From (23) and (27), an objective function that represents the improvement of the i th VF by measurements of the j th target can be formulated as follows:

$$J_{ij} \triangleq w_{ij} \sum_{\ell=k}^{k_f} (1-\gamma) \gamma^{\ell-k} I(\mathbf{v}_i; \mathbf{z}_j(\ell)) P(\mathbf{s}(\ell), \mathbf{x}_j(\ell)) \quad (28)$$

for $i = 1, \dots, M$, and $j = 1, \dots, N$. Then, the MO problem to be solved at time step k can be stated as follows:

$$\begin{aligned} \max \quad & [J_{11} \quad \dots \quad J_{MN}]^T \\ \text{sbj. to} \quad & \mathbf{s}(k) = \mathbf{s}_0 \\ & \mathbf{s}(\ell+1) = \mathbf{A}\mathbf{s}(\ell) + \mathbf{B}\mathbf{u}(\ell), \quad \ell = k, \dots, k_f \\ & \mathbf{b}_1 \leq \mathbf{s}(\ell) \leq \mathbf{b}_2, \quad \ell = k, \dots, k_f \\ & -\mathbf{1}_2 \leq \mathbf{u}(\ell) \leq \mathbf{1}_2, \quad \ell = k, \dots, k_f \end{aligned} \quad (29)$$

where \mathbf{s}_0 is the known state of the camera at time k . Because the state of the PT camera $\mathbf{s}(\ell+1)$ depends on the control input $\mathbf{u}(\ell)$, the variables of the above MO problems are as follows:

$$\boldsymbol{\chi} \triangleq [\mathbf{s}^T(k) \quad \dots \quad \mathbf{s}^T(k_f) \quad \mathbf{u}^T(k) \quad \dots \quad \mathbf{u}^T(k_f)]^T \quad (30)$$

The constraints on the camera states and control inputs in (29) can be expressed compactly as

$$\mathcal{U} \triangleq \{\boldsymbol{\chi} \in \mathbb{R}^{6T} \mid \mathbf{C}\boldsymbol{\chi} = \mathbf{d}_1, \mathbf{D}\boldsymbol{\chi} \leq \mathbf{d}_2\} \quad (31)$$

where

$$\mathbf{C} \triangleq \begin{bmatrix} \mathbf{I}_4 & \mathbf{0} & \mathbf{0} & \dots & \mathbf{0} & \mathbf{0} & \dots & \dots & \mathbf{0} \\ -\mathbf{A} & \mathbf{I}_4 & \mathbf{0} & \dots & \mathbf{0} & \mathbf{B} & \mathbf{0} & \dots & \mathbf{0} \\ \mathbf{0} & -\mathbf{A} & \mathbf{I}_4 & \ddots & \vdots & \mathbf{0} & \mathbf{B} & \ddots & \vdots \\ \vdots & \ddots & \ddots & \ddots & \mathbf{0} & \vdots & \ddots & \ddots & \mathbf{0} \\ \mathbf{0} & \dots & \mathbf{0} & -\mathbf{A} & \mathbf{I}_4 & \mathbf{0} & \dots & \mathbf{0} & \mathbf{B} \end{bmatrix}$$

$\underbrace{\hspace{10em}}_{4T} \qquad \underbrace{\hspace{10em}}_{2T}$

$$\mathbf{d}_1 \triangleq [\mathbf{s}_0^T \quad \mathbf{0}_{1 \times 4(k-1)}]^T, \quad \mathbf{D} \triangleq \begin{bmatrix} -\mathbf{I}_{4T} & \mathbf{I}_{4T} & \mathbf{0}_{4T \times 4T} \\ \mathbf{0}_{2T \times 8T} & -\mathbf{I}_{2T} & \mathbf{I}_{2T} \end{bmatrix}^T$$

$$\mathbf{d}_2 \triangleq \left[\underbrace{\mathbf{b}_1^T \dots \mathbf{b}_1^T}_{4T} \quad \underbrace{\mathbf{b}_2^T \dots \mathbf{b}_2^T}_{2T} \quad \mathbf{1}_{1 \times 4T} \right]^T \quad (32)$$

\mathbf{I}_n is an $n \times n$ identity matrix, and $\mathbf{0}_{m \times n}$ and $\mathbf{1}_{m \times n}$ denote $m \times n$ matrices of zeros and ones, respectively.

Assume the MN objective functions defined in (28) can be arranged in an ordered set $\{J'_1, \dots, J'_R\}$, where objective J'_j is more important than J'_i if $j < i$ ($j \neq i$), for all $j, i = \{1, \dots, R\}$, $R = MN$. Then, the lexicographic approach obtains the solution to the MO problem in (29) by solving a sequence of single-objective optimization problems

$$\max_{\boldsymbol{\chi}} J'_i(\boldsymbol{\chi}) \quad (33a)$$

$$\text{sbj. to } J'_j(\boldsymbol{\chi}) \geq (J'_j)^*, \quad j = 1, \dots, i-1, \quad i > 1 \quad (33b)$$

$$\boldsymbol{\chi} \in \mathcal{U} \quad (33c)$$

$$i = 1, \dots, R \quad (33d)$$

where $(J'_j)^*$ is the optimum of the j th objective function, found in the j th iteration [41].

For the PT camera MO problem in (29), the above ordering assumption can be satisfied as follows. From (28), J_{ij} denotes the expected improvement in the i th VF brought about by measurements obtained from the j th target. Let the order notation $J_{ij} \succ J_{i'j'}$ ($J_{ij} \prec J_{i'j'}$) denote an objective J_{ij} that is more (less) important than $J_{i'j'}$ ($\forall i' \neq i$ and $\forall j' \neq j$). For a given target j , objective functions corresponding to higher target-VF association probabilities (21) are more important because they correspond to a higher target detection probability, thus

$$J_{ij} \succ J_{i'j} \Leftrightarrow w_{ij} \geq w_{i'j}, \quad 1 \leq i \neq i' \leq M \quad (34)$$

and the M objective functions can be rearranged in order of decreasing importance, such that

$$J_{1j} \succ J_{2j} \succ \dots \succ J_{Mj}, \quad j = 1, \dots, N. \quad (35)$$

Also, for different targets ($j \neq j'$) objective functions corresponding to smaller VF indices are considered more important because learned earlier in the observation process, thus

$$J_{ij} \succ J_{i'j'}, \quad 1 \leq i < i' \leq M, \quad 1 \leq j \neq j' \leq N \quad (36)$$

and combining (35) and (36) leads to the order

$$J_{ij} \succ J_{i'j'}, \quad 1 \leq i < i' \leq M, \quad 1 \leq j, j' \leq N. \quad (37)$$

In the special case $i = i'$, the relative importance of objectives cannot be determined by the target-VF association probability. Let \check{J}_{ij} denote the objective value obtained by optimizing J_{ij} independently of the other objectives, or

$$\check{J}_{ij} \triangleq \max_{\boldsymbol{\chi}} \{J_{ij}(\boldsymbol{\chi}) | \boldsymbol{\chi} \in \mathcal{U}\}. \quad (38)$$

Then, for $i = i'$, it is reasonable to assume that objective functions corresponding to larger optima are more important, or

$$J_{ij} \succ J_{i'j'} \Leftrightarrow \check{J}_{ij} \geq \check{J}_{i'j'}, \quad 1 \leq j, j' \leq N \quad (39)$$

for $i = 1, \dots, M$. When combined, (37) and (39) completely specify the ordered set for the MO problem in (29), which can then be reduced to the sequence of single-objective optimization

problems

$$\max_{\boldsymbol{\chi}} J_{i'j'}(\boldsymbol{\chi}) \quad (40a)$$

$$\text{sbj. to } J_{ij}(\boldsymbol{\chi}) \geq J_{ij}^*, \quad \forall J_{ij} \prec J_{i'j'} \quad (40b)$$

$$\boldsymbol{\chi} \in \mathcal{U} \quad (40c)$$

$$i = 1, \dots, M, \quad j = 1, \dots, N \quad (40d)$$

where the optimum J_{ij}^* is known from the previous iteration. An efficient solution to the above single-objective optimization problems is presented in the next section.

B. Sequential Optimization of Information Objectives

Because the mutual information, $I(\mathbf{v}_i; \mathbf{z}_j(\ell))$, is not an explicit function of $\boldsymbol{\chi}$, the single-objective optimization problem in (40) is equivalent to maximizing a weighted sum of the potential functions, $P(\mathbf{s}(\ell), \mathbf{x}_j(\ell))$. Also, during the first iteration of the lexicographic method [$i = 1$ in (40)], the camera state and control inputs are only subject to the linear constraints (40c). In the weighted sum of potential functions in (28), choose the weight of the ℓ th potential function in J_{ij} to be

$$\beta(\ell) = w_{ij}(1 - \gamma)\gamma^{\ell-k} I(\mathbf{v}_i; \mathbf{z}_j(\ell)), \quad \ell = k, \dots, k_f.$$

Then, J_{ij} is a quadratic function of $\boldsymbol{\chi}$, because

$$\begin{aligned} J_{ij} &= \sum_{\ell=k}^{k_f} \beta(\ell) - \sum_{\ell=k}^{k_f} \frac{\beta(\ell)}{h} \|\mathbf{U}\mathbf{s}(\ell) - \mathbf{g}[\mathbf{x}_j(\ell)]\|^2 \\ &= \left(\sum_{\ell=k}^{k_f} \beta(\ell) - \mathbf{c}^T \mathbf{c} \right) - \left(\boldsymbol{\chi}^T \mathbf{P}^T \mathbf{P} \boldsymbol{\chi} - \mathbf{c}^T \mathbf{P} \boldsymbol{\chi} \right) \end{aligned} \quad (41)$$

where

$$\mathbf{P} \triangleq \begin{bmatrix} \sqrt{\frac{\beta(k)}{h}} \mathbf{U} & \mathbf{0} & \dots & \mathbf{0} \\ \mathbf{0} & \sqrt{\frac{\beta(k+1)}{h}} \mathbf{U} & \ddots & \vdots \\ \vdots & \ddots & \ddots & \mathbf{0} \\ \mathbf{0} & \dots & \mathbf{0} & \sqrt{\frac{\beta(k_f)}{h}} \mathbf{U} \end{bmatrix} \mathbf{0}_{2T \times 2T} \quad (42)$$

$$\mathbf{c} \triangleq \left[\sqrt{\frac{\beta(k)}{h}} \mathbf{g}^T[\mathbf{x}_j(k)] \dots \sqrt{\frac{\beta(k_f)}{h}} \mathbf{g}^T[\mathbf{x}_j(k_f)] \right]^T. \quad (43)$$

Hence, the first iteration of the lexicographic method can be solved by a QP algorithm, such as interior point, in polynomial time [48].

Subsequent iterations [$i > 1$ in (40)] can be cast in the form (41)–(43), with an added set of constraints (40b). Although the constraints in (40b) are nonlinear, they can be approximated by linear constraints with a bounded loss in performance, as shown in the remainder of this section. From the measurement model (2), if $\mathbf{x}_j(\ell) \in \mathcal{S}(\ell)$ at time ℓ , then $\mathbf{z}_j(\ell)$ is independent of $\boldsymbol{\chi}$. Because the cumulative EKLD bound in (23) is also independent of $\boldsymbol{\chi}$, the constraints in (40b) can be replaced by the following

T geometric constraints:

$$J_{ij}(\mathbf{x}) \geq J_{ij}^* \Leftrightarrow \begin{cases} \mathbf{x}_j(\ell) \in \mathcal{S}(\ell), & \mathbf{x}_j(\ell) \in \mathcal{S}^*(\ell), \\ \ell = k, \dots, k_f & \\ \text{unconstrained,} & \text{o.w.} \end{cases} \quad (44)$$

without decreasing the information value (23).

Because the target position, $\mathbf{x}_j \in \mathcal{W}$, is beyond our control, (44) translates into geometric constraints to be satisfied by the PT camera state and control (\mathbf{x}) and, in particular, by the camera pan and tilt angles, ψ and ϕ . Thus, in order to reduce the single-objective optimization problems in (40) to QP form, the nonlinear constraints (44) are approximated by a linear set as follows. In \mathcal{W} , the geometry of the FOV, $\mathcal{S}(\ell)$, is an irregular convex tetragon that changes with respect to time by virtue of the camera PT angles (see Fig. 1). When projected onto the virtual image plane (see Fig. 2), however, $\mathcal{S}(\ell)$ is a rectangle with the same size as the image sensor. Let a and b denote the width and height of the image sensor, respectively. Given that the projection of $\mathbf{x}_j(\ell)$ onto the virtual image plane \mathbf{p}_j is known from (5) and (6), it follows that $\mathbf{x}_j(\ell) \in \mathcal{S}(\ell)$ iff

$$\mathbf{p}_j = [p_x \quad p_y]^T \in [-a/2, a/2] \times [-b/2, b/2]. \quad (45)$$

Then, the relationship between the PT camera angles and the convex function defined by (26) and (27) is obtained by substituting (5) and (6) in (26)

$$\begin{cases} \phi - \phi_j \triangleq \phi'_j = -\tan^{-1}(p_y/\lambda) \\ \psi - \psi_j \triangleq \psi'_j = -\tan^{-1}[p_x \sec(\phi_j) \cos(\phi'_j)/\lambda] \end{cases} \quad (46)$$

and the analytical form of (44) is obtained by substituting (45) in (46) as follows:

$$\begin{cases} |\phi'_j| \leq \tan^{-1}[b/(2\lambda)] \triangleq \phi_\lambda \\ |\psi'_j| \leq \tan^{-1}\left[\frac{a}{2\lambda}|\sec(\phi_j)|\cos(\phi'_j)\right] \triangleq g(\phi'_j). \end{cases} \quad (47)$$

The above constraint is illustrated in Fig. 4 for $[\psi_j \quad \phi_j]^T = [\pi/2 \quad \pi/4]^T$.

Because the FOV constraint in (47) is proven to be convex by the following theorem, all iterations of the lexicographic method presented in this section require polynomial time.

Theorem 4: The FOV constraint (47) is convex with respect to the camera PT coordinates $[\psi \quad \phi]^T$, given any camera parameters $a, b, \lambda > 0$ and target PT coordinates $[\psi_j \quad \phi_j]^T$.

Proof: The inequalities in (47) can be rewritten as

$$\begin{cases} |\phi'_j| \leq \phi_\lambda \\ |\psi'_j| \leq g(\phi'_j) \end{cases} \quad (48)$$

a constraint equivalent to the intersection of the epigraph of $-g(\phi'_j)$ and the hypograph of $g(\phi'_j)$, for $\phi'_j \in [-\phi_\lambda, \phi_\lambda]$ (e.g., see Fig. 4), where the epigraph (hypograph) of a function is defined as the set of points lying on or above (below) its graph [49]. From (47), the second derivative of $g(\phi'_j)$ is

$$\frac{d^2 g(\phi'_j)}{d\phi'^2_j} = -\frac{g_0 \cos(\phi'_j)[1 + g_0^2 + g_0^2 \sin^2(\phi'_j)]}{[1 + g_0^2 \cos^2(\phi'_j)]^2} \quad (49)$$

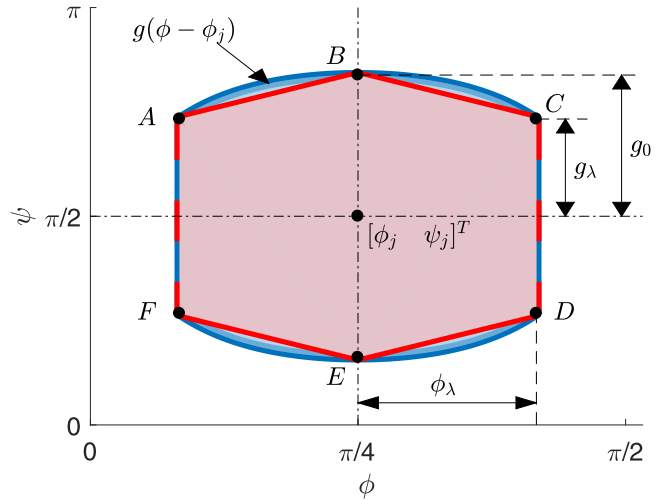


Fig. 4. Example of nonlinear constraint (47) (blue region bounded by arcs \widehat{ABC} , \widehat{DEF} , and segments \overline{CD} , \overline{FA}) and corresponding linear approximation (50) (polygon $ABCDEF$).

where $g_0 \triangleq g(0)$. Since g_0 is a positive constant, $d^2 g/d\phi'^2_j \leq 0$ for $\phi'_j \in [-\pi/2, \pi/2]$. Also, since $b, \lambda > 0$, it follows that $0 < \phi_\lambda < \pi/2$. Therefore, $g(\phi'_j)$ and $-g(\phi'_j)$ are concave and convex functions of ϕ'_j , respectively, where $\phi'_j \in [-\phi_\lambda, \phi_\lambda]$. Because the epigraph (hypograph) of a function is a convex set, if the function is a convex (concave) function [50], then the epigraph of $-g(\phi'_j)$ and the hypograph of $g(\phi'_j)$ are both convex sets. Finally, since the intersection of two convex sets is also a convex set, the intersection of the epigraph of $-g(\phi'_j)$ and the hypograph of $g(\phi'_j)$ is a convex set. ■

The computational complexity of the camera MO problem is further reduced by approximating the convex FOV constraint in (47) by the set of linear constraints

$$\begin{cases} |\phi'_j| \leq \phi_\lambda \\ |\psi'_j| \leq g_0 \pm \frac{[g_0 - g(\phi_\lambda)]}{\phi_\lambda} \phi'_j \end{cases} \quad (50)$$

accompanied by a bounded loss in performance. The above linear approximation is illustrated in Fig. 4, where it can be seen that ϕ_λ is half of the vertical angle of view with respect to the focal length λ . Then, letting the minimum focal length be $\lambda_m > 0$, ϕ_λ is characterized by the upper bound

$$\phi_\lambda \leq \tan^{-1}[b/(2\lambda_m)] \triangleq \phi_u \quad (51)$$

and the performance loss brought about by replacing (47) with (50) is guaranteed to be bounded by approximately 9% as proven by the following theorem and remarks.

Theorem 5: The ratio of the area of the camera FOV represented by the linear constraint (50) over the area of the FOV represented by the convex constraint (47) is bounded below by

$$r(\phi_u) \triangleq 1 - \frac{1}{4} \left[\sqrt{\left(\frac{\pi}{\phi_u} - 2\right)} - \sqrt{\frac{\pi}{\phi_u}} \right]^2 \quad (52)$$

where ϕ_u is a camera parameter defined in (51).

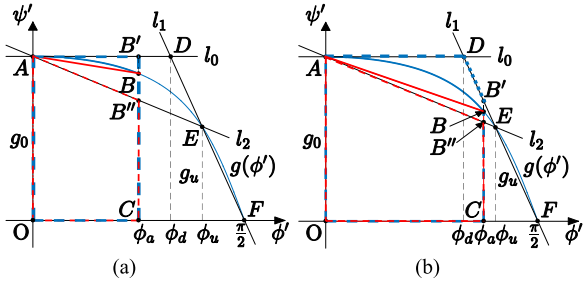


Fig. 5. Linear approximation (50) of nonlinear constraint (47) in the first quadrant when (a) $\phi_\lambda \leq \phi_d$ and (b) $\phi_\lambda > \phi_d$, where polygons of area S_1 and S_2 are denoted by blue and red dashed lines, respectively.

Proof: Since (48) and (50) are symmetric about both the ϕ'_j and ψ'_j axes, the ratio of the area of (50) over the area of (48) is the same as the area ratio in the first quadrant: $\{(\phi'_j, \psi'_j) | \phi'_j \geq 0, \psi'_j \geq 0\}$. Let point A denote the intersection between the ψ'_j -axis and $g(\phi'_j)$ (see Fig. 5). Let point E denote the pair $(\phi_u, g(\phi_u))$, where ϕ_u is the upper bound of ϕ'_j . Now, let S_1 denote the area of the convex set specified by the nonlinear constraint (48) in the first quadrant (blue dashed line in Fig. 5), and line l_0 denote a horizontal line through A , as illustrated in Fig. 5. The first derivative of $g(\phi'_j)$ is

$$dg(\phi'_j)/d\phi'_j = -g_0 \sin \phi'_j / (g_0^2 \cos^2 \phi'_j + 1) \leq 0 \quad (53)$$

for all $\phi'_j \in [0, \pi/2]$. Therefore, $g(\phi'_j)$ is monotonically decreasing for all $\phi'_j \in [0, \pi/2]$, and is bounded above by l_0 . Let l_1 denote a line through points E and F , defined graphically in Fig. 5. Since $g(\phi'_j)$ is a concave function for all $\phi'_j \in [0, \pi/2]$ (see Theorem 4), $g(\phi'_j)$ is bounded above by line l_1 for all $\phi'_j \in [0, \phi_u]$. Let point D denote the intersection of lines l_0 and l_1 , and let ϕ_d denote the ϕ'_j -axis coordinate of point D . Then, if $\phi_\lambda \leq \phi_d$, S_1 is bounded above by the area of polygon $OAB'C$ [dashed blue line in Fig. 5(a)], and if $\phi_\lambda > \phi_d$, S_1 is bounded above by the area of polygon $OADB'C$ [dashed blue line in Fig. 5(b)], or

$$S_1 \leq \begin{cases} g_0 \phi_\lambda, & \text{if } \phi_\lambda \leq \phi_d \\ g_0 \phi_d + \frac{1}{2}(g_\lambda + g_0)(\phi_\lambda - \phi_d), & \text{if } \phi_\lambda > \phi_d \end{cases} \quad (54)$$

where $g_0 \triangleq g(0)$ and $g_\lambda \triangleq g(\phi_\lambda)$.

Now, let S_2 denote the area of the convex set specified by the linear constraints (50) in the first quadrant. Let l_2 denote a line through points A and E , defined graphically in Fig. 5. Since $g(\phi'_j)$ is a concave function in $[0, \pi/2]$, it is bounded below by line l_2 for all $\phi'_j \in [0, \phi_u]$, and S_2 is greater than the area of polygon $OAB''C$ or

$$S_2 \geq \frac{(g_\lambda + g_0)}{2} \phi_\lambda = \left[\frac{(g_u - g_0)}{2\phi_u} \phi_\lambda + g_0 \right] \phi_\lambda \quad (55)$$

where $g_u \triangleq g(\phi_u)$. For $\phi_\lambda \leq \phi_d$, substitute (55) into (54) such that the area ratio satisfies the inequality

$$\frac{S_2}{S_1} \geq 1 - \frac{(g_0 - g_u)}{2g_0 \phi_u} \phi_\lambda \quad (56)$$

and since $\phi_\lambda \leq \phi_d$ and $g_0 \geq g_u$, it also follows that

$$\begin{aligned} \frac{S_2}{S_1} &\geq 1 - \frac{(g_0 - g_u)}{2g_0 \phi_u} \phi_d \\ &= 1 - \frac{(g_0 - g_u)}{2g_0 \phi_u} \left[\frac{\pi}{2} - \left(\frac{\pi}{2} - \phi_u \right) \frac{g_0}{g_u} \right] \\ &= 1 + \frac{(1 - g_u/g_0)(\pi - 2\phi_u)}{g_u/g_0 \cdot 4\phi_u} - \frac{(1 - g_u/g_0)}{4\phi_u} \pi \\ &= 1 - c_1 - c_2 + c_1 \frac{g_0}{g_u} + c_2 \frac{g_u}{g_0} \end{aligned} \quad (57)$$

where $c_1 \triangleq (\pi - 2\phi_u)/(4\phi_u) > 0$ and $c_2 = \pi/(4\phi_u) > 0$ are known constants.

From (57), it can be shown that the area ratio satisfies

$$\begin{aligned} \frac{S_2}{S_1} &\geq 1 - c_1 - c_2 + 2\sqrt{c_1 c_2} = 1 - (\sqrt{c_1} - \sqrt{c_2})^2 \\ &= 1 - \frac{1}{4} \left(\sqrt{\left(\frac{\pi}{\phi_u} - 2 \right)} - \sqrt{\frac{\pi}{\phi_u}} \right)^2 \end{aligned} \quad (58)$$

and that the derivative of the lower bound in (58) with respect to ϕ_u is

$$\frac{d}{d\phi_u} \left(\frac{S_2}{S_1} \right) = -\frac{\pi}{4\phi_u^2} \frac{[\sqrt{(\pi - 2\phi_u)} - \sqrt{\pi}]^2}{\sqrt{(\pi - 2\phi_u)\pi}} \leq 0 \quad (59)$$

where equality holds for $\phi_u = \pi/2$.

For $\phi_\lambda > \phi_d$, the area ratio satisfies the inequality

$$\frac{S_2}{S_1} \geq \left\{ \frac{g_0}{\left[\frac{(g_u - g_0)}{2\phi_u} \phi_\lambda + g_0 \right] \phi_\lambda} + \left(1 - \frac{\phi_d}{\phi_\lambda} \right) \right\}^{-1} \quad (60)$$

where the right-hand side is a monotonically increasing function of ϕ_λ and, thus

$$\begin{aligned} \frac{S_2}{S_1} &\geq \left\{ \frac{g_0}{\left[\frac{(g_u - g_0)}{2\phi_u} \phi_d + g_0 \right]} \right\}^{-1} = 1 - \frac{(g_0 - g_u)}{2g_0 \phi_u} \phi_d \\ &\geq 1 - \frac{(g_0 - g_u)}{2g_0 \phi_u} \phi_u. \end{aligned} \quad (61)$$

Then, similarly to (56), it can be shown that

$$\frac{S_2}{S_1} \geq 1 - \frac{1}{4} \left[\sqrt{\left(\frac{\pi}{\phi_u} - 2 \right)} - \sqrt{\frac{\pi}{\phi_u}} \right]^2 \quad (62)$$

because $g(\phi'_j)$ is a monotonically decreasing function of ϕ'_j , for all $\phi'_j \in [0, \pi/2]$. Finally, the area ratio bounds in (58) and (62) are met in the limit of $\lambda \rightarrow \infty$ when $\phi_\lambda = \phi_d$. ■

Remark 1: $r(\phi_u)$ is a monotonically decreasing function of ϕ_u for all $\phi_u \in [0, \pi/2]$.

Remark 2: For a PT camera with a vertical angle of view $\phi_u < \pi/4$, the lower bound on the FOV area ratio obeys $r(\phi_u) > r(\pi/4) = 1 - \frac{(\sqrt{2}-1)^2}{2} \approx 91.4\%$.

Based on Theorem 5 and Remark 2, the optimization problems in (40) can each be formulated as QP problems with objective function (41) and linear constraints (50). Then, the optimal

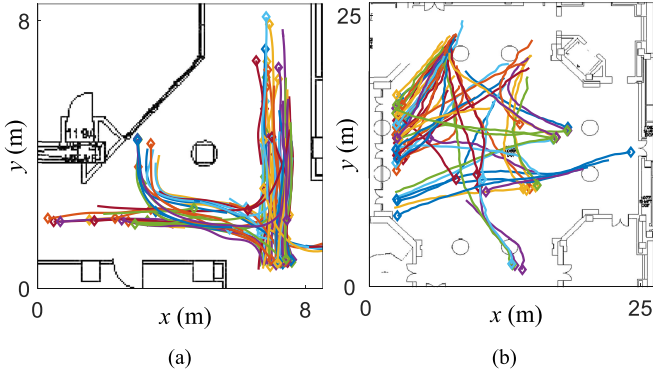


Fig. 6. Two experimental datasets consisting of time-stamped sequences of position and velocity measurements of pedestrians at a frequency of 2 Hz. Initial positions are denoted by diamonds. (a) Dataset I: 88 pedestrians measured at the intersection of two corridors. (b) Dataset II: 61 pedestrians measured in a lobby area.

Algorithm 1: Lexicographic Algorithm for k th Time Step.

- 1: Given \mathbf{C} , \mathbf{D} , \mathbf{d}_1 , \mathbf{d}_2 , and $\{J_{ij}, w_{ij}\}_{i,j}$
 - 2: **for** $j = 1, \dots, N$ **do**
 - 3: Sort $\{w_{ij}\}_i$ such that $w_{1j} \geq w_{2j} \geq \dots \geq w_{Mj}$
 - 4: Order J_{1j}, \dots, J_{Mj} according to sorted $\{w_{ij}\}_i$
 - 5: **end for**
 - 6: $\mathcal{U} \leftarrow \{\chi \in \mathbb{R}^{6T} \mid \mathbf{C}\chi = \mathbf{d}_1, \mathbf{D}\chi \leq \mathbf{d}_2\}$
 - 7: **for** $i = 1, \dots, M$ **do**
 - 8: Sort $\{\check{J}_{ij}\}_j$, such that $\check{J}_{i1} \geq \check{J}_{i2} \geq \dots \geq \check{J}_{iN}$
 - 9: Rearrange $\{J_{ij}\}_j$ according to sorted $\{\check{J}_{ij}\}_j$
 - 10: **for** $j = 1, \dots, N$ **do**
 - 11: $\chi^* \leftarrow \arg \max_{\chi} \{J_{ij}(\chi) \mid \chi \in \mathcal{U}\}$
 - 12: **for** $\ell = k, \dots, k_f$ **do**
 - 13: **if** $\mathbf{x}_j(\ell) \in \mathcal{S}[\mathbf{s}^*(\ell)]$ **then**
 - 14: $\mathcal{V} \leftarrow \{\chi \mid |\phi(\ell) - \phi_j(\ell)| \leq \phi_\lambda,$
 $|\psi(\ell) - \psi_j(\ell)| \leq g_0 \pm \frac{g_0 - g_\lambda}{\phi_\lambda} (\phi - \phi_j)\}$
 - 15: $\mathcal{U} \leftarrow \mathcal{U} \cap \mathcal{V}$
 - 16: **end if**
 - 17: **end for**
 - 18: **end for**
 - 19: **end for**
 - 20: **end for**
 - 21: **return** χ^*
-

PT camera state and control sequence χ^* can be obtained efficiently by the lexicographic method in Algorithm 1. Unlike the original camera control problem, Algorithm 1 can be implemented in polynomial time and is applicable in real time with a performance loss described by Remark 2.

VI. SIMULATIONS AND RESULTS

In this section, the EKLD lower bound \hat{D}_L derived in closed form in Theorem 3, and used to obtain the MO objective functions in (28), is first verified for a variety of target kinematics (see Section VI-A). Then, in Section VI-B, the effectiveness of the lexicographic method (see Algorithm 1) is demonstrated in

TABLE I
PT CAMERA PARAMETERS

Description	Variable	Value
Horizontal angle of view	g_0	45°
Vertical angle of view	ϕ_u	32°
Maximum pan angular velocity	$\dot{\psi}_m$	$100^\circ/\text{s}$
Maximum tilt angular velocity	$\dot{\phi}_m$	$100^\circ/\text{s}$
Motor coefficients	b_1, b_2	$100^\circ/(\text{Vs}^2)$
Covariance matrix	\mathbf{Q}	$0.1 \mathbf{I}_4$ (m), (m/s)

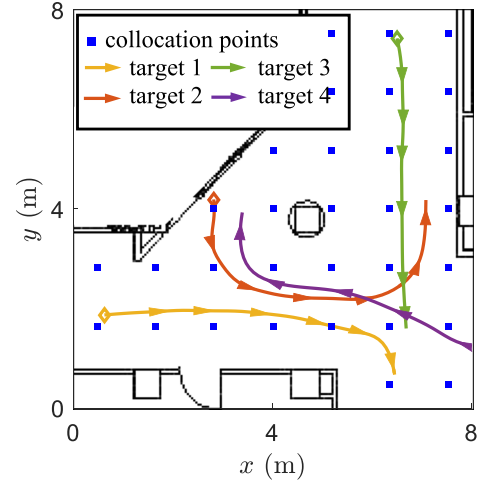


Fig. 7. Four examples of targets from Dataset I in Fig. 6(a) superimposed with the collocation points.

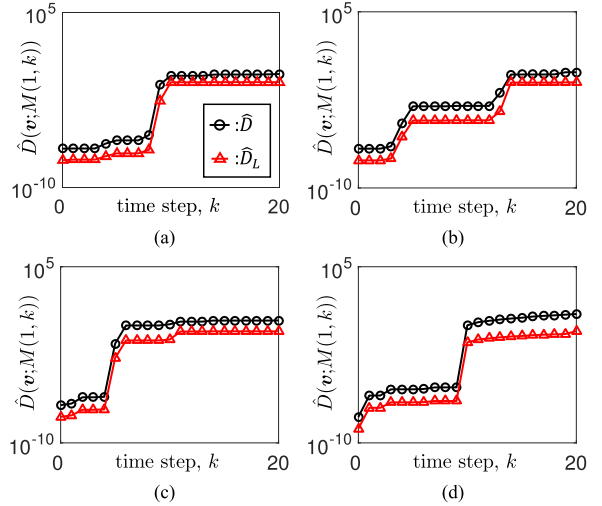


Fig. 8. Comparison between the cumulative lower bound (23) (red line with triangles), and the DPGP-EKLD (18) (black line with circles). Panels (a)–(d) correspond to targets 1–4 in Fig. 7, respectively.

simulations and compared to the optimal solution obtained offline, and to solutions obtained by existing algorithms based on entropy reduction [19], greedy [20], potential field [21], patrol [22], and random [17] methods. For all of these methods, the camera constraints are taken into account. Finally, the computational complexity of the lexicographic algorithm and of the

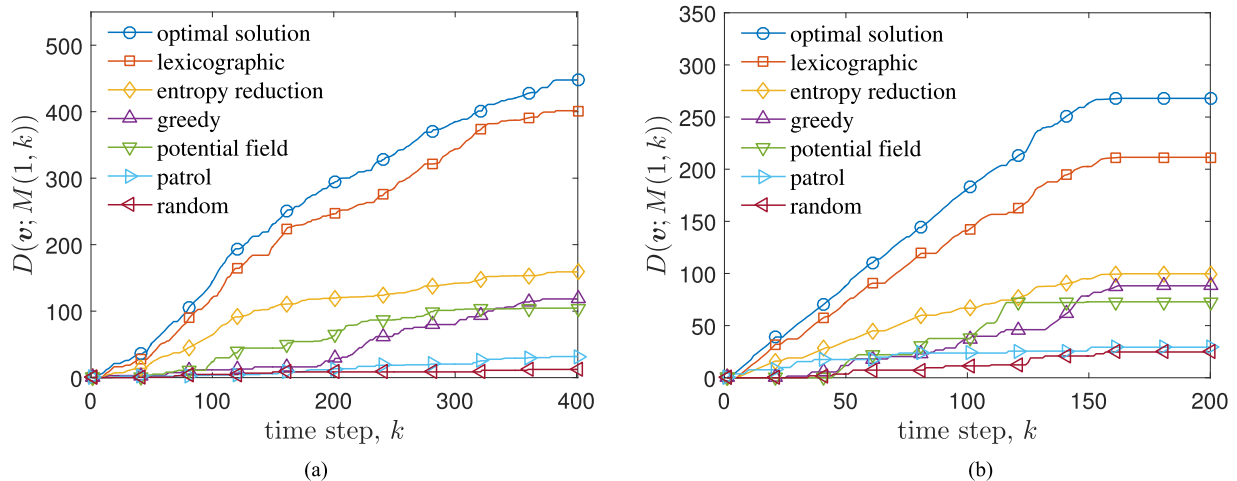


Fig. 9. DPGP KL divergence obtained by the seven camera control algorithms for (a) pedestrian dataset I [see Fig. 6(a)] and (b) pedestrian dataset II [see Fig. 6(b)].

other six algorithms is analyzed theoretically and tested experimentally in Section VI-C.

The simulations are performed using two experimental datasets obtained by PT cameras observing pedestrians inside MIT buildings [10], as shown in Fig. 6. For each of the two experimental datasets, 75% of the pedestrians measurements are selected at random and introduced as the targets in the simulations, and the remaining 25% of the pedestrian measurements are used as test datasets to evaluate the performance of the DPGP camera control algorithms. The PT camera is assumed to be located above the center of the workspace. Camera parameters are adopted from commercial PT cameras, such as the AXIS M5013 Dome Network camera [51], and are summarized in Table I.

A. EKLD Lower Bound Simulation Results

The distance between the DPGP-EKLD (18) and its lower bound (23) is evaluated for four targets shown in Fig. 7. Both the EKLD and its lower bound are calculated using the squared-exponential covariance function

$$\Psi(\mathbf{x}, \mathbf{x}') = \exp\left(-\frac{\|\mathbf{x} - \mathbf{x}'\|^2}{2l^2}\right) \mathbf{I}_2 \quad (63)$$

where $l = 1$ is the characteristic length scale. The collocation points are distributed on a uniform grid in \mathcal{W} . The discount factor in (23) controls the shape of the cumulative lower bound. Larger values of γ make the cumulative lower bound follow the trend of the DPGP-EKLD more closely and, therefore, in this paper $\gamma = 0.9$ in all simulations. Studies using other length scales and discount values were also performed but produced similar results and, therefore, are omitted for brevity. The results in Fig. 8 show that \hat{D}_L in (23) is typically lower than \hat{D} in (18) by a constant distance on a logarithm scale, for all four targets in Fig. 7. This distance is approximately equal to the factor $(1 - \gamma)$ in the EKLD lower bound (23), thus confirming that the bound can be maximized in lieu of the original (nonadditive) EKLD function (18).

TABLE II
RMSEs OF DPGP-MMs

Algorithms	Dataset I	Dataset II
All data	8.97%	9.03%
Optimal solution [14]	9.12%	9.58%
Lexicographic	9.15%	10.88%
Entropy reduction [19]	16.25%	18.52%
Greedy [20]	15.68%	17.89%
Potential field [21]	29.72%	30.21%
Patrol [22]	27.47%	40.17%
Random [17]	92.81%	93.51%

B. Lexicographic Camera Control Results

The effectiveness of the lexicographic method is compared to that of five existing algorithms referred to as entropy reduction [19], greedy [20], potential field [21], patrol [22], and random [17] algorithms. The entropy reduction algorithm decides the next camera state by maximizing the DPGP expected entropy reduction of the next measurement, $\mathbf{z}_j(k)$, for one time step [19]. The greedy algorithm maximizes the DPGP-EKLD of $\mathbf{z}_j(k)$, shown in (18), for one time step using a computationally efficient particle-filter-based search method presented in [20]. The entropy and greedy algorithms do not take into account the PT camera constraints but only the next measurement value. The potential field algorithm, inspired by [21], controls the camera movement by building attracting fields centered at estimates of the target states projected onto the PT space. The patrol algorithm taken from [22] adopts a sliding-mode-based method to predefine a fixed route for the camera.

The random algorithm generates multiple number of random control trajectories based on an extension of the rapidly exploring random tree in [17], and chooses the control trajectory with the highest DPGP-EKLD. Then, the camera control inputs are determined by solving a nonlinear programming problem with the greedy DPGP-EKLD in (18) as objective function. The optimal camera control solution is obtained offline, for

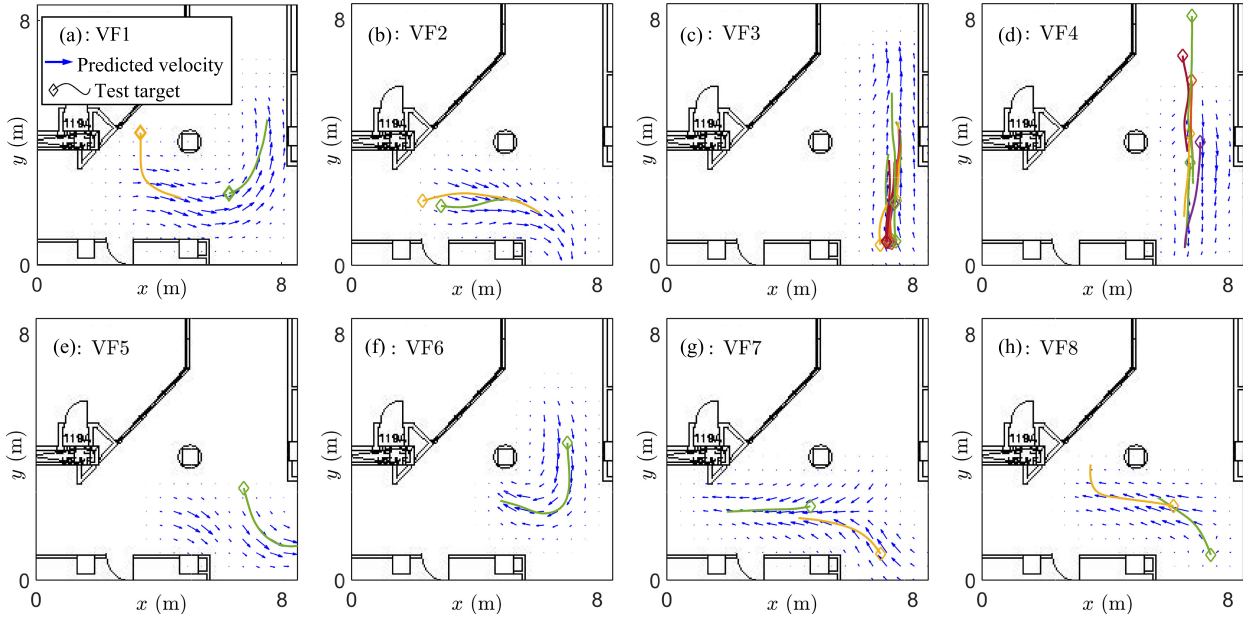


Fig. 10. Target kinematic models (VFs with the highest likelihood) learned by the lexicographic algorithm at the final time are superimposed on actual trajectories of test targets for the pedestrian dataset I in Fig. 6(a).

comparison, by maximizing the cumulative DPGP-EKLD in (18) over the entire time horizon $[k, k_f]$ using the sequential quadratic programming (SQP) algorithm implemented by the MATLAB optimization toolbox *fmincon* function [52]. Although too computationally intensive for real-time applications (see Section VI-C), the optimal solution is useful in assessing the performance of the lexicographic algorithm presented in this paper.

After the measurements are obtained by all seven algorithms, the *actual* DPGP KL divergence, $D(\mathbf{v}; Z(1, k))$ in (16), is evaluated and used to compare their performance. The time histories of the DPGP KL divergence for all seven algorithms are plotted in Fig. 9, using the datasets in Fig. 6, and the camera parameters in Table I. It can be seen from Fig. 9 that the lexicographic algorithm developed in this paper achieves the highest information value of all algorithms, with the exception of the optimal solution. Furthermore, these results show that the performance of the lexicographic algorithm is very close to that of the optimal solution (obtained offline).

In order to evaluate the accuracy of the DPGP model of target kinematics learned by the camera control algorithms at the final time k_f (with $T = 400$ or 200), the root-mean-square error (RMSE) of the DPGP-MM is evaluated as follows. Let K_j denote the number of measurements obtained from the j th pedestrian in each of the two test datasets, and let $\hat{\mathbf{v}}_j$ represent the j th target velocity estimated from the DPGP-MM (as shown in [14]). Then, the RMSE is defined as follows:

$$\epsilon = \frac{1}{N_{\text{tot}}} \sum_{j=1}^{N_T} \sum_{i=1}^M w_{ij} \sqrt{\frac{1}{K_j} \sum_{k=1}^{K_j} \frac{\|\mathbf{v}_j(k) - \hat{\mathbf{v}}_j(k)\|^2}{\|\mathbf{v}_j(k)\|^2}} \quad (64)$$

where the *total* number of targets in the test dataset, N_{tot} , is used in lieu of N , because N is a function of time.

The RMSEs obtained for all seven camera control algorithms, using the pedestrian datasets I and II shown in Fig. 6, are summarized in Table II. The case referred to as “all data” is one where all available measurements of the pedestrian movements are used for learning the DPGP-MMs and, thus, is characterized by the lowest possible error achievable by any camera control algorithm. Although not physically realizable by a single camera, the results for this case are included in Table II for comparison. The results in Table II show that the DPGP-MMs learned from the measurements obtained by the optimal solution and the lexicographic algorithm are the most accurate. As additional validation, the VFs learned by the lexicographic method at the final time of the simulation for dataset I are plotted in Fig. 10, superimposed on the actual trajectories of the test targets. These results provide a visual verification that the target kinematics learned from the lexicographic camera measurements are very close to the ground truth.

C. Computational Complexity Analysis

Because solving the PT camera control problem optimally was proven to be NP-hard in Section IV-A, the computational complexity of the proposed lexicographic algorithm is analyzed in this section and compared to that of the five existing algorithms tested in Section VI-B. The complexity of the lexicographic algorithm is dominated by the calculations of the cumulative lower bounds (23), which require $O(L^2T)$ time for every target and every VF, where L is the number of collocation points (defined in Section III), and T is the number of steps in the time horizon (defined in Section IV-A). Each single-objective quadratic optimization in (40) takes $O(T^3)$ time. Therefore, the computational complexity of the lexicographic method is $O((L^2 + T^2)MNT)$, where M is the number of VFs and N is the number of targets in the workspace.

TABLE III
COMPUTATIONAL COMPLEXITY

Algorithms	Theoretical complexity	Experimental complexity (sec)	
		Dataset I	Dataset II
Optimal solution	NP -hard	16.014	15.092
Lexicographic	$O((L^2 + T^2)MNT)$	0.081	0.073
Entropy reduction	$O((L^2 + T^2)MNT)$	0.077	0.072
Greedy	$O([L^2 + \log(MN)]MN)$	0.044	0.044
Potential field	$O(L^2MN)$	0.003	0.003
Patrol	$O(1)$	< 0.001	< 0.001
Random	$O(L^2MNT)$	0.002	0.002

The computational complexity of the other six algorithms was also analyzed for comparison and the results are summarized in Table III (individual analysis omitted for brevity). Table III also shows the computation times obtained experimentally for all seven algorithms on a Dell Precision T7400 workstation, with a 3.20 GHz Intel(R) Xeon(R) CPU, and 16.0 GB installed memory. It can be seen from both the theoretical and experimental results that the computational complexity of the lexicographic method is much lower than that of the optimal solution. Although other algorithms require less computation, the lexicographic algorithm affords much higher performance and can be easily implemented in real time. Hyper-parameter optimizations and sparsifications of the GPs may also be performed during the DPGP-MM update to further reduce the computation time if deemed necessary by other applications.

VII. CONCLUSION

The problem of learning the behavior of many moving targets by means of a reconfigurable camera is relevant to a wide range of applications, including security and surveillance, environmental monitoring, and tracking of endangered species. Information value functions based on the KL divergence have been shown the most effective for planning future measurements using greedy strategies. However, when utilized to optimally control a sensor subject to kinematic and FOV constraints, the resulting problem is NP-hard. This paper presents a new additive lower bound on the cumulative information value that significantly reduces computational complexity while providing satisfactory performance guarantees. Based on the results in this paper, the camera control problem can be solved as a sequence of quadratic programs by a lexicographic approach. Extensive tests involving real pedestrian data show that this approach is applicable in real time and is significantly more effective than existing methods based, for example, on greedy entropy reduction, greedy KL divergence, potential field, patrol, and randomly exploring trees.

REFERENCES

- [1] H. Wei and S. Ferrari, "A geometric transversals approach to analyzing the probability of track detection for maneuvering targets," *IEEE Trans. Comput.*, vol. 63, no. 11, pp. 2633–2646, Nov. 2014.
- [2] H. Wei and S. Ferrari, "A geometric transversals approach to sensor motion planning for tracking maneuvering targets," *IEEE Trans. Automat. Control*, vol. 60, no. 10, pp. 2773–2778, Oct. 2015.
- [3] A. Singh, F. Ramos, H. D. Whyte, and W. J. Kaiser, "Modeling and decision making in spatio-temporal processes for environmental surveillance," in *Proc. IEEE Int. Conf. Robot. Autom.*, 2010, pp. 5490–5497.
- [4] G. Foderaro, P. Zhu, H. Wei, T. A. Wettergren, and S. Ferrari, "Distributed optimal control of sensor networks for dynamic target tracking," *IEEE Trans. Control Netw. Syst.*, vol. 5, no. 1, pp. 142–153, Mar. 2018.
- [5] G. Aoude, B. D. Luders, J. Joseph, N. Roy, and J. P. How, "Probabilistically safe motion planning to avoid dynamic obstacles with uncertain motion patterns," *Auton. Robots*, vol. 35, no. 1, pp. 51–76, 2013.
- [6] X. Wang, K. Tieu, and E. Grimson, "Learning semantic scene models by trajectory analysis," in *Computer Vision—ECCV 2006*. New York, NY, USA: Springer, 2006, pp. 110–123.
- [7] S. Reece *et al.*, "Gaussian process segmentation of co-moving animals," *AIP Conf. Proc.—Amer. Inst. Phys.*, vol. 1305, no. 1, pp. 430–437, 2011.
- [8] C. E. Rasmussen, "The infinite Gaussian mixture model," in *Proc. Adv. Neural Inf. Process. Syst.*, Denver, CO, USA, Dec. 1999, vol. 12, pp. 554–560.
- [9] J. Joseph, F. Doshi-Velez, A. S. Huang, and N. Roy, "A Bayesian non-parametric approach to modeling motion patterns," *Auton. Robots*, vol. 31, no. 4, pp. 383–400, 2011.
- [10] Y. F. Chen, M. Liu, S.-Y. Liu, J. Miller, and J. P. How, "Predictive modeling of pedestrian motion patterns with Bayesian nonparametrics," in *Proc. AIAA Guid., Navig., Control Conf.*, 2016, pp. 1861–1874.
- [11] M. Schwager, B. J. Julian, and D. Rus, "Optimal coverage for multiple hovering robots with downward facing cameras," in *Proc. IEEE Int. Conf. Robot. Autom.*, 2009, pp. 3515–3522.
- [12] C. Ding, A. A. Morye, J. A. Farrell, and A. K. Roy-Chowdhury, "Coordinated sensing and tracking for mobile camera platforms," in *Proc. IEEE Amer. Control Conf.*, 2012, pp. 5114–5119.
- [13] A. A. Morye, E. Franco, A. K. Roy-Chowdhury, and J. A. Farrell, "Distributed camera control via moving horizon Bayesian optimization," in *Proc. IEEE Amer. Control Conf.*, 2014, pp. 2083–2089.
- [14] H. Wei *et al.*, "Information value in nonparametric Dirichlet-process Gaussian-process (DPGP) mixture models," *Automatica*, vol. 74, pp. 360–368, 2016.
- [15] A. Krause, A. Singh, and C. Guestrin, "Near-optimal sensor placements in Gaussian processes: Theory, efficient algorithms and empirical studies," *J. Mach. Learn. Res.*, vol. 9, pp. 235–284, 2008.
- [16] J. L. Ny and G. J. Pappas, "On trajectory optimization for active sensing in Gaussian process models," in *Proc. IEEE Conf. Decis. Control*, Shanghai, China, Dec. 2009, pp. 6286–6292.
- [17] C. Fulgenzi, C. Tay, A. Spalanzani, and C. Laugier, "Probabilistic navigation in dynamic environment using rapidly-exploring random trees and Gaussian processes," in *Proc. IEEE/RSJ Int. Conf. Intell. Robots Syst.*, 2008, pp. 1056–1062.
- [18] P. Zhu, H. Wei, W. Lu, and S. Ferrari, "Multi-kernel probability distribution regressions," in *Proc. IEEE Int. Joint Conf. Neural Netw.*, 2015, pp. 1–7.
- [19] P. Salvagnini *et al.*, "Information theoretic sensor management for multi-target tracking with a single pan-tilt-zoom camera," in *Proc. IEEE Winter Conf. Appl. Comput. Vis.*, 2014, pp. 893–900.

- [20] H. Wei *et al.*, "Camera control for learning nonlinear target dynamics via Bayesian nonparametric Dirichlet-process Gaussian-process (DP-GP) models," in *Proc. IEEE/RSJ Int. Conf. Intell. Robots Syst.*, 2014, pp. 95–102.
- [21] W. Lu, G. Zhang, and S. Ferrari, "An information potential approach to integrated sensor path planning and control," *IEEE Trans. Robot.*, vol. 30, no. 4, pp. 919–934, Aug. 2014.
- [22] A. S. Matveev, H. Teimoori, and A. V. Savkin, "A method for guidance and control of an autonomous vehicle in problems of border patrolling and obstacle avoidance," *Automatica*, vol. 47, no. 3, pp. 515–524, 2011.
- [23] Mathworks, Natick, MA, USA, Matlab Computer Vision Toolbox, 2016. [Online]. Available: <http://www.mathworks.com>
- [24] N. Gans, G. Hu, and W. Dixon, "Keeping multiple objects in the field of view of a single PTZ camera," in *Proc. IEEE Amer. Control Conf.*, 2009, pp. 5259–5264.
- [25] J. Heikkilä, "Geometric camera calibration using circular control points," *IEEE Trans. Pattern Anal. Mach. Intell.*, vol. 22, no. 10, pp. 1066–1077, Oct. 2000.
- [26] A. P. Dani, N. R. Fischer, and W. E. Dixon, "Single camera structure and motion," *IEEE Trans. Automat. Control*, vol. 57, no. 1, pp. 238–243, Jan. 2012.
- [27] R. Tron and R. Vidal, "Distributed 3-D localization of camera sensor networks from 2-D image measurements," *IEEE Trans. Automat. Control*, vol. 59, no. 12, pp. 3325–3340, Dec. 2014.
- [28] O. Avni, F. Borrelli, G. Katzir, E. Rivlin, and H. Rotstein, "Scanning and tracking with independent cameras: A biologically motivated approach based on model predictive control," *Auton. Robots*, vol. 24, no. 3, pp. 285–302, 2008.
- [29] S. N. Vukosavic, *Digital Control of Electrical Drives*. New York, NY, USA: Springer, 2007.
- [30] K. Wang, J. Chiasson, M. Bodson, and L. M. Tolbert, "A nonlinear least-squares approach for identification of the induction motor parameters," *IEEE Trans. Automat. Control*, vol. 50, no. 10, pp. 1622–1628, Oct. 2005.
- [31] G. Aoude, J. Joseph, N. Roy, and J. How, "Mobile agent trajectory prediction using Bayesian nonparametric reachability trees," in *Proc. AIAA Infotech@Aerosp.*, 2011, pp. 1587–1593.
- [32] C. E. Rasmussen and C. Williams, *Gaussian Processes for Machine Learning*. Cambridge, MA, USA: MIT Press, 2006.
- [33] H. Wei, W. Lu, and S. Ferrari, "An information value function for nonparametric Gaussian processes," arXiv preprint arXiv:1406.3296, 2014.
- [34] F. Nobile, R. Tempone, and C. G. Webster, "A sparse grid stochastic collocation method for partial differential equations with random input data," *SIAM J. Numer. Anal.*, vol. 46, no. 5, pp. 2309–2345, 2008.
- [35] H. Wei, W. Lu, P. Zhu, G. Huang, J. Leonard, and S. Ferrari, "Optimized visibility motion planning for target tracking and localization," in *Proc. IEEE/RSJ Int. Conf. Intell. Robots Syst.*, 2014, pp. 76–82.
- [36] H. Wei, "Non-parametric Bayesian models for decentralized sensor path planning," Ph.D. dissertation, Dept. Mech. Eng. Mater. Sci., Duke Univ., 2016.
- [37] T. Cover and J. Thomas, *Elements of Information Theory*. New York, NY, USA: Wiley-Interscience, 1991.
- [38] C.-W. Ko, J. Lee, and M. Queyranne, "An exact algorithm for maximum entropy sampling," *Oper. Res.*, vol. 43, no. 4, pp. 684–691, 1995.
- [39] M. R. Garey and D. S. Johnson, *Computers and Intractability*. San Francisco, CA, USA: Freeman, 2002.
- [40] C. Scherer, P. Gahinet, and M. Chilali, "Multiobjective output-feedback control via LMI optimization," *IEEE Trans. Automat. Control*, vol. 42, no. 7, pp. 896–911, Jul. 1997.
- [41] R. T. Marler and J. S. Arora, "Survey of multi-objective optimization methods for engineering," *Struct. Multidiscip. Optim.*, vol. 26, no. 6, pp. 369–395, 2004.
- [42] A. Messac, "From dubious construction of objective functions to the application of physical programming," *AIAA J.*, vol. 38, no. 1, pp. 155–163, 2000.
- [43] A. Messac and C. A. Mattson, "Generating well-distributed sets of Pareto points for engineering design using physical programming," *Optim. Eng.*, vol. 3, no. 4, pp. 431–450, 2002.
- [44] K. A. Proos, G. Steven, O. Querin, and Y. Xie, "Multicriterion evolutionary structural optimization using the weighting and the global criterion methods," *AIAA J.*, vol. 39, no. 10, pp. 2006–2012, 2001.
- [45] N. Bezzo, R. Fierro, A. Swingler, and S. Ferrari, "A disjunctive programming approach for motion planning of mobile router networks," *Int. J. Robot. Autom.*, vol. 26, no. 1, 2011.
- [46] A. Swingler and S. Ferrari, "A cell decomposition approach to cooperative path planning and collision avoidance via disjunctive programming," in *Proc. 49th IEEE Conf. Decis. Control*, 2010, pp. 6329–6336.
- [47] S. Ferrari, C. Cai, R. Fierro, and B. Perteet, "A multi-objective optimization approach to detecting and tracking dynamic targets in pursuit-evasion games," in *Proc. Amer. Control Conf.*, New York, NY, USA, Jul. 11–13, 2007, pp. 5316–5321.
- [48] A. Hansson, "A primal-dual interior-point method for robust optimal control of linear discrete-time systems," *IEEE Trans. Automat. Control*, vol. 45, no. 9, pp. 1639–1655, Sep. 2000.
- [49] T. Abburi and S. Narasimhan, "Optimal sensor scheduling in batch processes using convex relaxations and Tchebycheff systems theory," *IEEE Trans. Automat. Control*, vol. 59, no. 11, pp. 2978–2983, Nov. 2014.
- [50] M. Giaquinta and G. Modica, *Mathematical Analysis: Foundations and Advanced Techniques for Functions of Several Variables*. New York, NY, USA: Springer, 2011.
- [51] Axis Communications, Lund, Sweden, "Product comparison tables, network video," 2015. [Online]. Available: http://www.axis.com/files/cheat_sheets/chs_62583_us_r5_1503_lo.pdf
- [52] Mathworks, Natick, MA, USA, Matlab Optimization Toolbox, function: fmincon, 2004. [Online]. Available: <http://www.mathworks.com>



Hongchuan Wei received the Master's of Science degree in computer science and Ph.D. degree in mechanical engineering and materials science from Duke University, Durham, NC, USA, in 2013 and 2016, respectively.

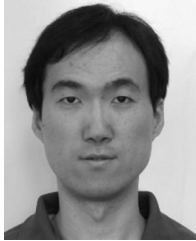
His current research focuses on sensor network deployment, which consists of optimally placing a set of sensors in a region of interest (ROI) such that the probability of detection of targets traveling through the ROI is maximized.

The probability of detection is a function of the target movement and sensors field of view. He is also interested in utilizing information theoretic functions to acquire optimal sensor controls in order to learn the behaviors of targets described by nonparametric Bayesian models.



Pingping Zhu (S'10–M'13) received the B.S. degree in electronics and information engineering and M.S. degree from the Institute for Pattern Recognition and Artificial Intelligence, Huazhong University of Science and Technology, Wuhan, China, in 2006 and 2008, respectively, and the M.S. and Ph.D. degrees in electrical and computer engineering from the University of Florida, Gainesville, FL, USA, in 2010 and 2013, respectively.

He is currently a Research Associate with the Department of Mechanical and Aerospace Engineering, Cornell University, Ithaca, NY, USA. Prior to that, he was a Postdoctoral Associate with the Department of Mechanical Engineering and Material Science, Duke University. His research interests include approximate dynamic programming, optimal control of mobile sensor networks, finite random set statistics (FISST), signal processing, machine learning, and neural networks.



Miao Liu received the B.S. and M.S. degrees in electronics and information engineering from Huazhong University of Science and Technology, Wuhan, China, in 2005 and 2007, respectively, and the Ph.D. degree in electrical and computer engineering from Duke University, Durham, NC, USA, in 2014.

He is currently a Research Staff Member with the AI Science Department at the Machine Learning for Artificial Intelligence Foundations Group, IBM T. J. Watson Research Center, Yorktown Heights, NY, USA. Before that, he was a Postdoctoral Associate with the Laboratory of Information and Decision System, Massachusetts Institute of Technology, where he was working on scalable Bayesian non-parametric methods for solving decentralized multiagent learning and planning problems. His research interests include statistical machine learning, and AI and robotics.



Silvia Ferrari (S'01–M'02–SM'08) received the B.S. degree from Embry-Riddle Aeronautical University, Daytona Beach, FL, USA, in 1997, and the M.A. and Ph.D. degrees from Princeton University, Princeton, NJ, USA, in 1998 and 2002, respectively.

She is currently a Professor of mechanical and aerospace engineering with Cornell University, Ithaca, NY, USA, and the Director of the Laboratory for Intelligent Systems and Controls. Her research interests include robust adaptive control of aircraft, learning and approximate dynamic programming, and optimal control of mobile sensor networks.

Dr. Ferrari is a member of ASME, SPIE, and AIAA. She was the recipient of the ONR Young Investigator Award (2004), the NSF CAREER Award (2005), and the Presidential Early Career Award for Scientists and Engineers Award (2006).



Jonathan P. How (F'18) received the B.A.Sc. degree in aerospace option from the University of Toronto, Toronto, ON, Canada, in 1987, and the S.M. and Ph.D. degrees in aeronautics and astronautics from the Massachusetts Institute of Technology (MIT), Cambridge, MA, USA, in 1990 and 1993, respectively.

He then studied for two years at MIT as a Postdoctoral Associate for the Middeck Active Control Experiment that flew onboard the Space Shuttle Endeavour in March 1995. Prior to joining MIT in 2000, he was an Assistant Professor with the Department of Aeronautics and Astronautics, Stanford University. He is currently the Richard C. Maclaurin Professor of aeronautics and astronautics with the MIT.

Prof. How is the Editor-in-Chief for the IEEE CONTROL SYSTEMS MAGAZINE and an Associate Editor for the *AIAA Journal of Aerospace Information Systems*. He was the recipient of the 2002 Institute of Navigation Burka Award, a Boeing Special Invention Award in 2008, the IFAC Automatica Award for best applications paper in 2011, the AeroLion Technologies Outstanding Paper Award for the *Journal Unmanned Systems* in 2015, won the IEEE Control Systems Society Video Clip Contest in 2015, and was also the recipient of the AIAA Best Paper in Conference Awards in 2011, 2012, and 2013. He was a coauthor of the paper that won the Best Student Paper award at IROS 2017. He is a Fellow of AIAA.